Peer-reviewed version available at *Atmosphere* **2020**, *11*, 177; doi:10.3390/atmos11020177

Article

Co-existance of Lightning Generated Whistlers, Hiss and Lower Hybrid Noise Observed by e- POP (SWARM-E) –RRI

Ashanthi Maxworth [1]*, Mark Gołkowski [2] and Glenn Hussey [1]

[1] Physics and Engineering Physics, University of Saskatchewan Canada;
[2] Electrical Engineering, University of Colorado Denver
* Correspondence: asm468@mail.usask.ca (A.M.)

Abstract: Whistler mode waves play a major role in regulating the lifetime of trapped electrons in the Earth's radiation belts. Specifically, whistler mode hiss waves are one of the mechanisms that maintains the slot region between the inner and outer radiation belts. The generation mechanism of hiss is a topic still under debate with at least three prominent theories present in the literature. Lightning generated whistlers in their ducted or non-ducted modes, are considered to be one of the possible sources of hiss. We present a study of new observations from the Radio Receiver Instrument (RRI) on the Enhanced Polar Outflow Probe (ePOP: currently known as SWARM-E). RRI consists of two orthogonal dipole antennas, which enables polarization measurements, when the satellite boresight is parallel to the geomagnetic field. Here we present 75 passes of ePOP - RRI from 2014 - 2018, in which lightning whistlers and hiss waves were observed. In more than 50% of those passes hiss is found to co-exist with the lightning whistlers. Moreover, the whistler observations are correlated with observations of wave power at the lower-hybrid resonance. The observations and a whistler mode ray-tracing study suggest that multiple-hop lightning induced whistlers can be a source of hiss and plasma instabilities in the magnetosphere.

Keywords: lightning whistlers, hiss, e-POP, raytracing, radio-receiver, lower hybrid resonance

1. Introduction

Whistler mode waves play a dominant role in Earth's radiation belt energy dynamics. Hence lightning generated whistlers, chorus and hiss have been a topic of interest for the scientific research community for more than half a century [1–16]. Chorus, a naturally occurring type of a whistler mode wave, usually exists in two frequency bands, with a gap in wave energy at around half the electron cyclotron frequency. According to the general consensus, chorus waves originate outside the plasmapause, around the magnetic equator and are driven by the pitch angle anisotropy[17–21]. Hiss, on the other hand, is less discrete in time, covers a wider bandwidth, and the source mechanism is still a topic of debate. In early work it was proposed that hiss is generated by lightning generated whistlers[6,22–24]. This mechanism was supported by satellite observations as well as raytracing studies. Another proposed concept posits that hiss is generated by the same nonlinear process from temperature anisotropy as chorus[8,25]. Other authors have proposed that hiss is generated in the plasma plume region and there are also hiss sources within the plasmasphere. [26–29]. The third, and perhaps most widely accepted theory today, is that hiss is sourced from chorus waves that have undergone multiple magnetospheric reflections and propagated into the plasmasphere. This notion has also been supported by observational evidence and raytracing studies[30–33]. However, recently the prevalence of the chorus-to-hiss mechanism was challenged by [34] who analyzed observations

on the Van Allen Probes spacecraft. In all likelihood, none of the above mentioned mecahnisms are mutually exclusive and there can be multiple competing sources of these waves. In this context it is also worth mentioning that lightning induced whistlers are also observed to sometimes trigger chorus waves [35].

Whistler mode waves have been observed on the ground as well as on satellites [16,28,36–40]. In this work, we present new observations of lightning whistlers and hiss observed by the enhanced Polar Outflow Probe (ePOP) Radio Receiver Instrument (RRI)[41–43]. During the time from January 2014 to December 2018, RRI has observed lightning generated whistlers in 75, 4-min passes. Out of those around 50% of the time whistler mode hiss was also observed. One other important observation is the presence of significant wave power at the lower hybrid (LH) resonance frequency. LH waves were first observed by Parrot *et al.* [36], Brice and Smith [44,45]. The generation of lower hybrid waves from lightning whistlers has been analyzed by Lee and Kuo [46]. Interaction between high intensity whistlers and lightning generated sferics can amplify LH noise [46]. The presence of small scale density irregularities has also been highlighted as an important feature of LH observations [47,48]. Out of the 75 events in which we observe lightning generated whistlers, we have observed the lower hybrid resonance frequency 70% of the time showing a correlation between lightning activity and the production of LH waves.

The organization of this paper is as follows: in Section 2 we present observations of whistlers, hiss and LH observations from ePOP-RRI. In Section 3 we analyze the eccentricity of hiss for the cases presented in Section 2, followed by a ray-tracing study on the possibility of lightning generated whistlers being the source of hiss. In Section 5 we discuss the results and Section 6 concludes the paper.

2. Observations

We have categorized 75 passes of observations into four cases: 1) lightning generated whistlers co-existing with hiss, 2) multi-hop ducted whistlers filling the whistler band, 3) hiss observation in the absence of whistlers and 4) some special cases where the waves are not clearly classified. In this section we present multiple examples of the above 4 cases and all observations are tabulated in Table A1.

2.1. Co-existence of Whistlers and Hiss

Figure 1 shows two spectrograms of observations made by ePOP containing whistlers with hiss. These records also include observations of wave power at the LH frequency. Figure 1 (a) shows a 2-min record from June 19, 2015 wherein ducted whistlers are observed, with increasing dispersion with successive hops. The energy from whistlers below 2.5 kHz, is seen to add to pre-existing hiss wave energy in this band. In Figure 1 (a), an almost emission of LH wave energy is present initially at 7 kHz, after which it slightly increases to later gradually decrease to about 5 kHz at the end of the record. According to Lee and Kuo [46], intense whistlers can excite LH waves, which is clearly observed by the higher intensities of the whistlers near the LH frequency. And this whistler-LH interaction is the source of low frequency noise above the LH frequency.

Figure 1 (b) shows another observation of whistlers, hiss and LH frequency made by ePOP RRI on May 13, 2018. In this 4 min record fractional hop whistlers, characterized by less dispersion, are observed. A hiss-like band is present throughout the record, that appears to become more intense in the final 2-mins of the observation. Compared to the case presented in Figure 1 (a), the hiss bandwidth is about 1 kHz higher in this observation. And the LH frequency (15 kHz) is also higher compared to the previous case (7 kHz). The frequencies of terrestrial VLF transmitters at frequencies around $\sim$20 kHz also exhibit spectral broadening that has been identified to be a LH phenomenon [49].

Preprints (www.preprints.org) | NOT PEER-REVIEWED | Posted: 11 January 2020 doi:10.20944/preprints202001.0103.v1

Peer-reviewed version available at Atmosphere 2020, 11, 177; doi:10.3390/atmos11020177

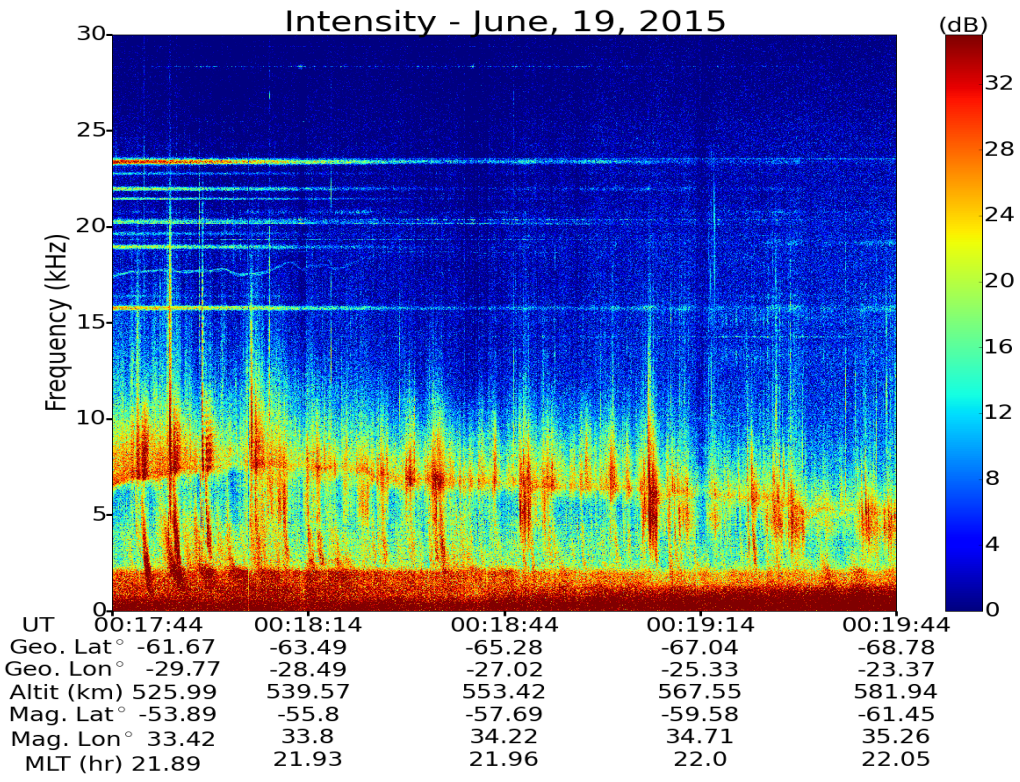

(a)

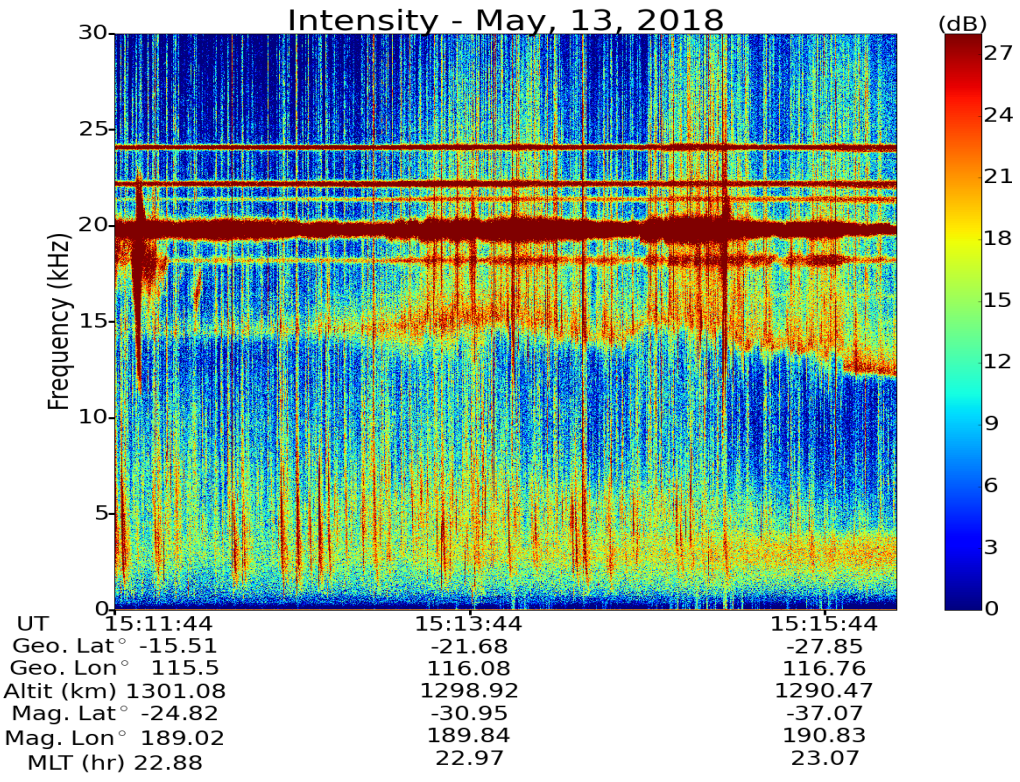

(b)

Figure 1. RRI frequency–time (f–t) spectrograms of signal intensity of whistlers co-exisiting with hiss and lower hybrid (LH) frequency. (a) ducted whistlers, hiss and LH frequency spectra observed by RRI on June 19, 2015. (b) lighting generated fractional-hop whistlers, hiss and LH waves observed on May 13, 2018. In addition to the natural low frequency waves the low frequency navy transmissions are also visible in both spectra.

2.2. Whistlers Appearing to Generate a Hiss Band

Figure 2 shows two observations of echoing ducted whistlers filling the hiss band. In Figure 2 (a), the observation was made by ePOP-RRI on February 19, 2014 and the figure shows only a 2-min portion. Figure 2 clearly shows the intensification of LH noise by the echoing whistlers (5 kHz - 15 kHz). In Figure 2 (a), the echoing whistlers fill the frequency band, $2 - 4kHz$ and the dispersion characteristics of whistlers are visible for about 90 seconds. With multiple echoes, the whistlers get more dispersed therefore they become more hiss-like with the scattered energy. Around 14:30:14 UT, there appears to be LH plasma turbulence, characterized by significant spectral broadening of the LH emission. This turbulence further intensified the LH noise around (10 kHz). This high intensified LH noise increases the entire noise level above and below the LH frequency. In the observed spectrogram, prior to the VLF turbulence, the noise level below LH is significantly lower compared to the noise level above it. Hence the LH frequency indirectly filters out the low frequency noise.

In the spectrogram shown in Figure 2 (b), the echoing whistlers are filling the hiss band frequencies below 2 kHz. In this observation also, the LH frequency is present starting at 4 kHz and increasing until 7 kHz. Throughout the spectrogram, whistler energy intensifies the hiss frequency band. Especially in the latter half of the observation, the echoing whistler structures are clearly visible below 2 kHz. Similar to the observation made in Figure 2 (a), in this case also, the echoing whistlers get more dispersed with each hop. With each echo, whistlers interact with LH waves, therefore the LH noise above the LH frequency gets intensified with each echo of whistlers.

2.3. Whistlers Interaction at the Lower Hybrid Resonace without Prominent Hiss

Figure 3 shows two spectrograms where there is a strong presence of LH frequency emissions without a prominent hiss band. In the spectrogram shown in Figure 3 (a), the LH frequency is centered around 5 kHz, and the noise level above it is significantly higher compared to the noise level below it. Although, there are lightning activity present above the LH frequency, the whistler activity is lower. An important observation of this spectrogram is the near absence of hiss.

On the observation made on July 28, 2018, shown in Figure 3 (b) similar features are observed with whistlers driving broadening of LH noise. In this observation the LH frequency starts around 5 kHz and gradually increases up to about 8 kHz. Weaker hiss emissions are seen around 1 kHz.

2.4. Hiss

Figure 4 shows an observation of magnetospheric hiss in the absence of whistlers. The lightning activity is visible but there are no observable lightning generated whistlers. It is important to note here, that this is the only example within 4 years worth of low frequency data of ePOP-RRI where only hiss is visible. In all the other cases, there are clear signatures of whistler activity in the presence of hiss. The LH frequency is also observed in the spectrogram around 5 kHz, but the intensity of the LH is low, compared to the previously presented cases.

2.5. More Complicated VLF Emissions

Figure 5 shows two examples of emissions in the ELF/VLF band that are harder to classify. The spectrogram presented in Figure 5 (a), shows structured emissions reminiscent of chorus observed on April 28, 2015. During the last three 2.5 mins of the spectrogram there are rising tone structures present in the frequency range 2 - 3.5 kHz. In this spectrogram also, the LH frequency emission is initially visible around 6 kHz, but the intensity of the LH noise is lower compared to the cases presented before. There is a general absence of whistler activity in this observation. Comparing this observation with the previously presented spectrograms in Figures 1, 2 and 3, we can make an assertion that LH emissions are significantly reduced in the absence of whistlers.

Figure 5 (b) shows another spectrogram of low frequency and LH frequency emissions made on January 19, 2016. In this observation also, there are few whistlers observed. But, the LH frequency

Preprints (www.preprints.org) | NOT PEER-REVIEWED | Posted: 11 January 2020 doi:10.20944/preprints202001.0103.v1

Peer-reviewed version available at Atmosphere 2020, 11, 177; doi:10.3390/atmos11020177

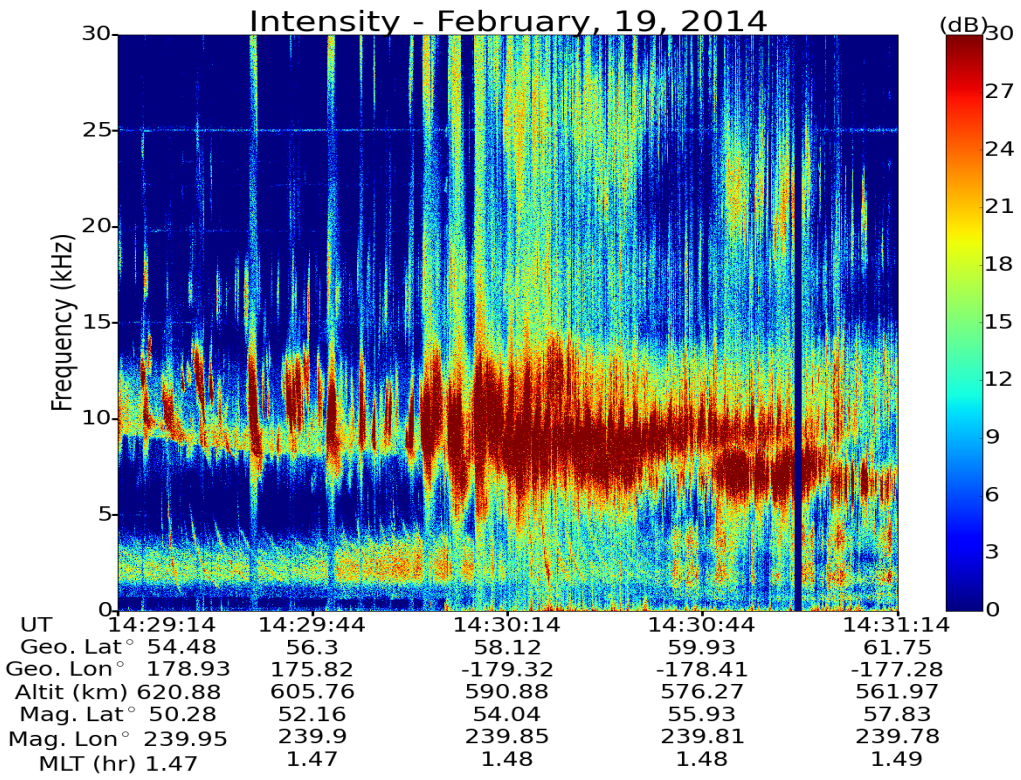

(a)

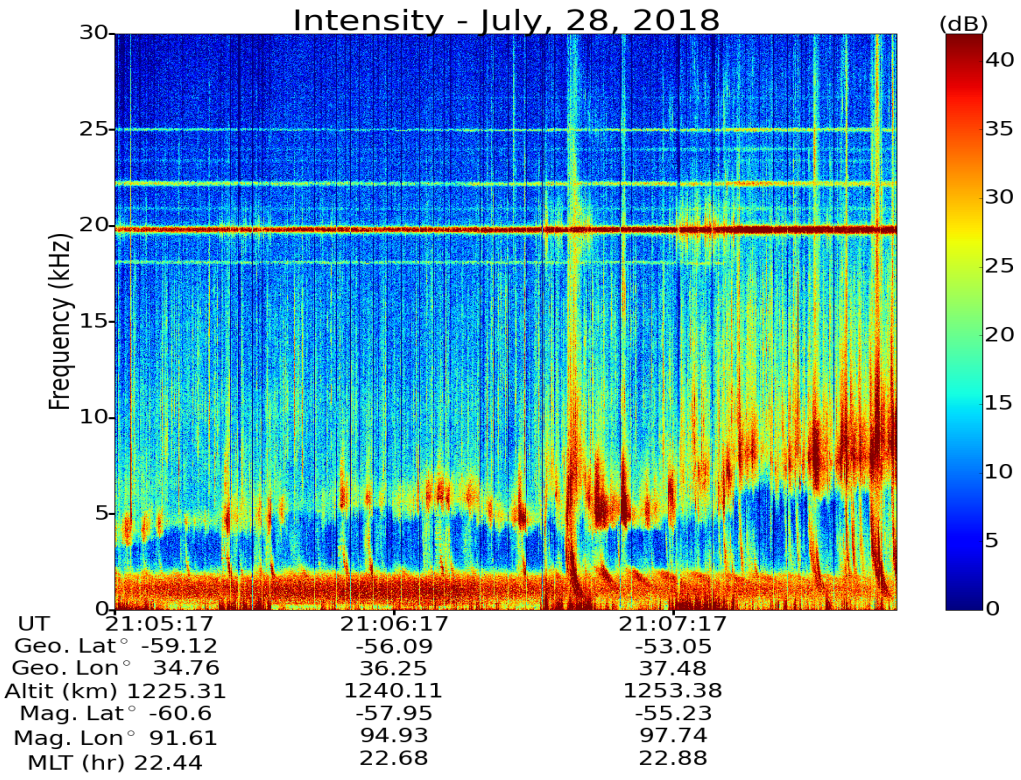

(b)

Figure 2. RRI frequency–time (f–t) spectrograms of signal intensity of ducted whistlers forming the hiss band. (a) multiple echoes of ducted whistlers are forming the hiss band observed on February 19, 2014. A low frequency plasma turbulence is observed around 14:30:14, and that increases the noise level above and beyond the LH frequency. (b) Multiple hops of ducted whistlers were observed on July 28, 2018. The echoing whistlers forming the hiss band is clearly visible during the last minute of the spectrogram. In both figures the interaction of whistlers amplifying the LH noise is clearly seen.

Preprints (www.preprints.org) | NOT PEER-REVIEWED | Posted: 11 January 2020 doi:10.20944/preprints202001.0103.v1

Peer-reviewed version available at Atmosphere 2020, 11, 177; doi:10.3390/atmos11020177

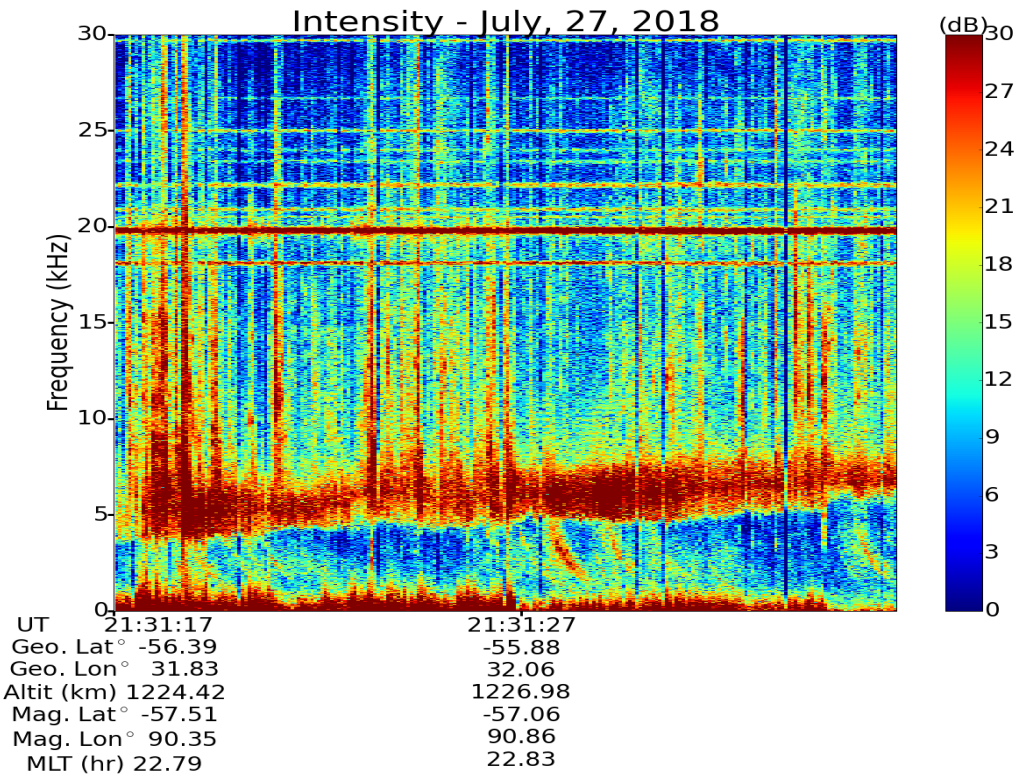

(a)

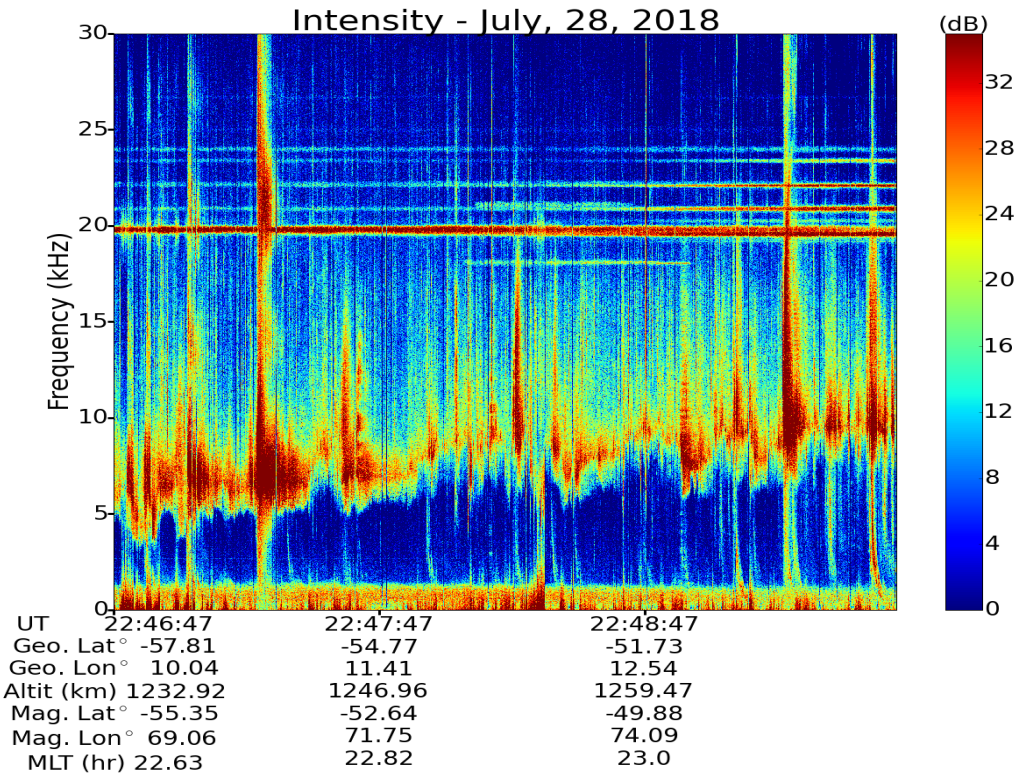

(b)

Figure 3. RRI frequency–time (f–t) spectrograms of signal intensity of lightning generated whistlers and lower hybrid resonance frequency. Hiss is not clearly visible in the spectra. (a) is a short ePOP flyover observed on July 27, 2018 where interaction of lightning generated whisters being the amplifier of low frequency noise and (b) shows amore clear event observed on July 28, 2018, in which the noise level below LH frequency is significantly lower than the noise level above it. In this case the LH frequency acts as noise filter, since majority of the lightning energy is being used for the amplification of LH noise, above the LH frequency.

Preprints (www.preprints.org) | NOT PEER-REVIEWED | Posted: 11 January 2020 doi:10.20944/preprints202001.0103.v1

Peer-reviewed version available at Atmosphere 2020, 11, 177; doi:10.3390/atmos11020177

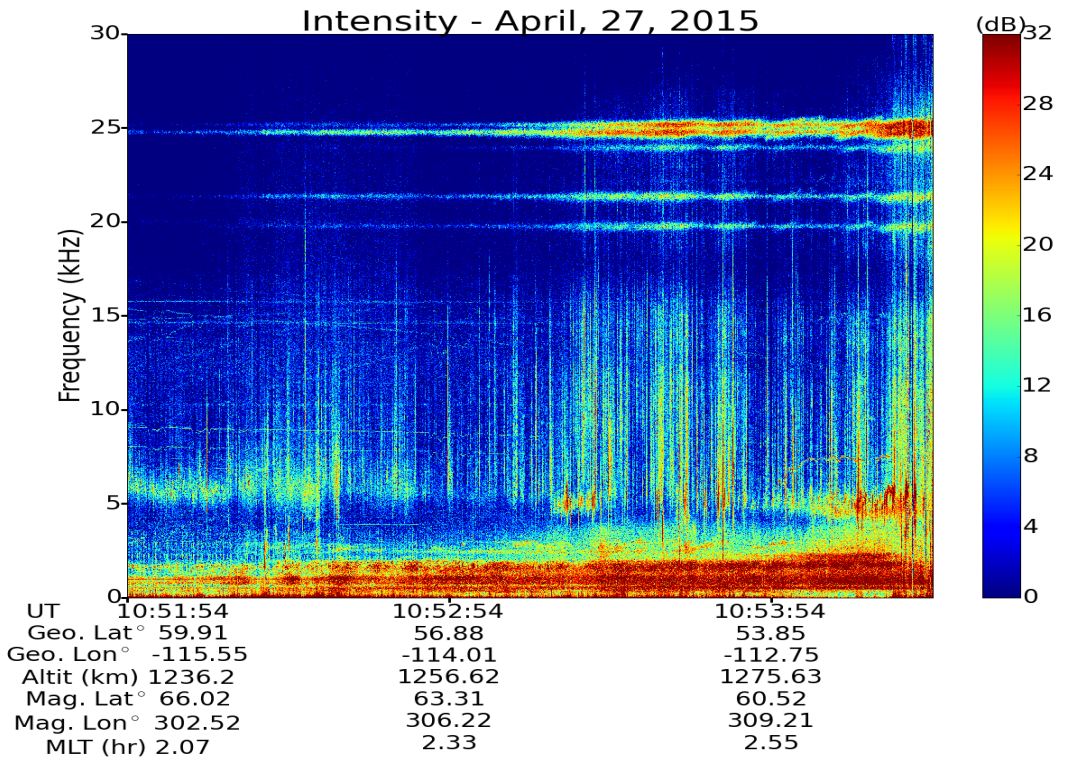

Figure 4. RRI frequency–time (f–t) spectrogram of hiss in the absence of whistlers observed on April 27, 2015. It is worth mentioning that, this is othe only clear example of hiss, in the absence of whistlers, within four years worth of ePOP- RRI data. The LH frequency is visible in the spectra, but the intensity of it is low compared to the intensity of hiss.

presented around 10 kHz is strong, and the VLF emissions extends up to 7 kHz. The VLF noise shows rising tone structures similar to quasi-periodic (QP) emissions of the type observed by Gołkowski and Inan [15]. There is some lightning activity observed around 9:27:14 UT and around 9:28:14 UT. At the time of those lightning events, the LH noise amplifies.

3. Eccentricity Analysis of Hiss

Based on the observations presented in Figure 2, echoing ducted whistlers can form a 1 -2 kHz hiss-band. Depending on the number of ducted whistlers and the background noise level, the composite signal structure might look very similar to the cases presented in Figure 1. Here we perform a brief eccentricity analysis of high frequency hiss (1 - 2 kHz) for the sample cases presented in Figures 1,2 and 4. For this analysis, we extracted amplitude maxima from the 2.5 mins observations of hiss from the frequency band 1 - 2 kHz, and calculated the eccentricity.

RRI consists of two orthogonal 6 m dipole antennas. When the RRI normal (boresight) is along the geomagnetic field, this configuration makes it easier to calculate the polarization parameters of the waves. RRI is capable of collecting in-phase and quadrature data from 10 Hz - 18 MHz. The bandwidth of the receiver is 30 kHz and the sampling rate is 62.5 kHz [41,42]. For this analysis, we have calculated the Stokes' parameters [50] and using those calculated the eccentricity of extracted high frequency hiss band, using the eccentricity equation given in Bass *et al.* [51]. The eccentricity presented here, is after averaging over all frequencies from 1-2 kHz and median filtered using sets of 21 samples.

According to Figure 6, the eccentricities of observed hiss from all cases, agree well with the previous studies [16] in which the eccentricity of magnetospheric whistler mode emissions is in the range of 0.8 - 0.9. The blue curve which represents hiss in the absence of whistlers, lies approximately marks the center of observations. The red curves represent the two cases where the whistlers were co-existing with pre-generated hiss and the green curves represent the cases where whistlers form the

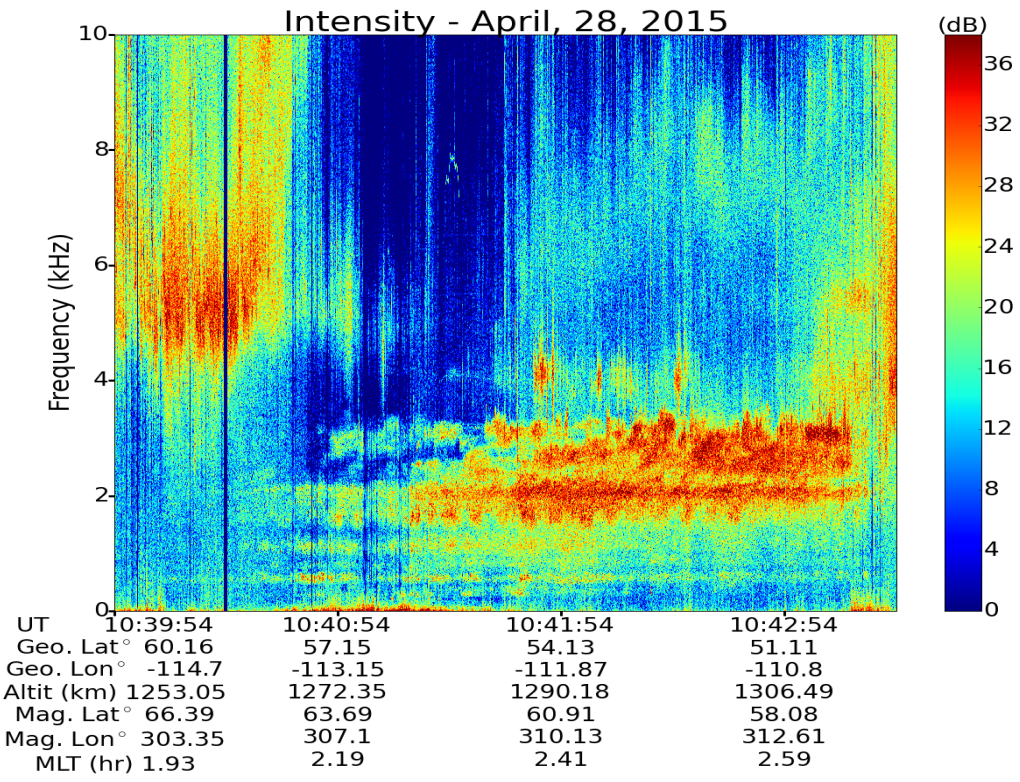

(a)

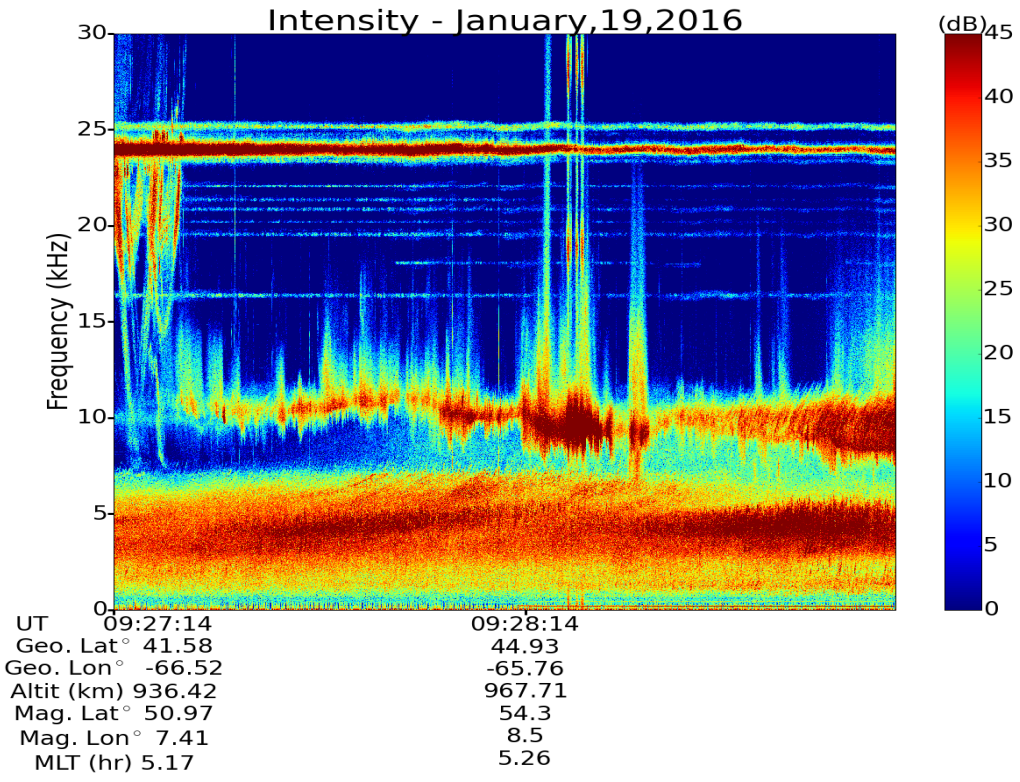

(b)

Figure 5. RRI frequency–time (f–t) spectrograms of signal intensity of low frequency waves observed by ePOP-RRI. (a) shows the zoomed in spectrogram of a low frequency structures observed on April 28, 2015. There are chorus-like structures in the second portion of the spectrogram, on top of the hiss-like signals. (b) shows a spectrogram of low frequency noise and a strong LH frequency from January 19, 2016. The low frequency noise structure is similar to QP emissions with very high frequency.

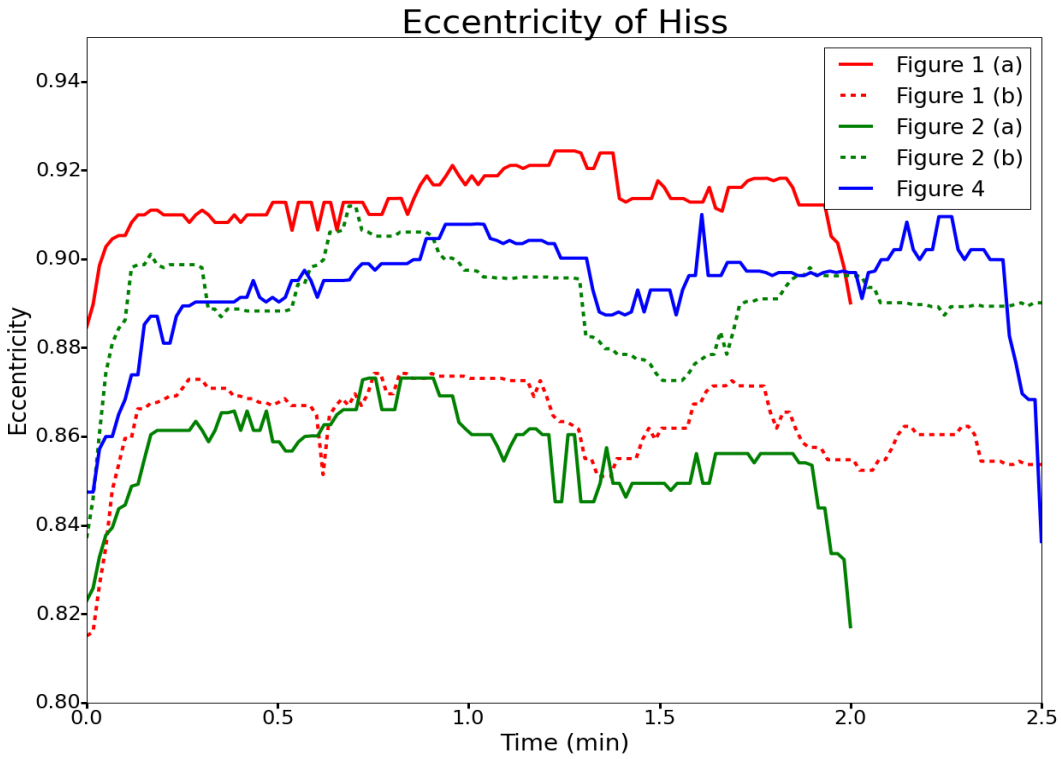

Figure 6. Eccentricity for the hiss in the frequency band 1 -2 kHz for the cases presented in Figures 1, 2 and 4. The eccentricity curve shown in blue is for the natural hiss shown in Figure 4 in the absence of whistlers. In other cases lightning generated whistlers are co-existing (or forming) hiss, therefore the the eccentricity shown here, the eccentricity of whistlers are included.

high frequency hiss band. From the eccentricity analysis, the dashed red curve (May 13, 2018) overlaps with the solid green curve (February 19, 2014). And there is an overlap between the dashed green curve (July 28, 2018) and the solid blue curve (April 27, 2015). For the first minute of observations there is agreement between the solid red curve (June 19, 2015) and the dashed green curve (July 28, 2018). This analysis shows that the difference between hiss, hiss existing with whistlers and whistlers filling the hiss band, is minimal.

4. Raytracing Results

In Figure 2 above, two cases were shown in which lightning generated ducted whistlers were echoing to fill the hiss frequency band. And Table A1, in the Appendix shows all whistler observations made by ePOP-RRI from 2014 to 2018. The number of whistler observations were high in 2018, because in that year the authors of this paper requested ePOP observations in the very low frequency range. In the previous years, the low frequency band observations were more random. We performed a raytracing study to observe the scattering nature of the whistlers into hiss.

In this work we launched 10,332 waves from 500 Hz to 4 kHz, with increments of 100 Hz, and with initial angles from 0° to 40° from vertical with 1° increments from geographic latitudes 0° to 30°(in 5° increments). It is important to note here that on the raytracer the launching angles are specified from the vertical axis, hence the launching angles and the wave normal angles are the same only at the equator. At all the other latitudes the wave normal angle is different from the launching angle depending on the angle of the geomagnetic field. All waves are traced until the power of the wave reached $-10dB$ from the initial power. We traced the wave normal angle along each wave trajectory.

From the simulation results we produced the frequency- time spectrogram from the simulations shown in Figure 7. The spectrogram in Figure 7 shows the simulated data points passing through a $1200km \times 1200km$ square cross section, with its bottom edge located at the equator and extending

Preprints (www.preprints.org) | NOT PEER-REVIEWED | Posted: 11 January 2020 doi:10.20944/preprints202001.0103.v1

Peer-reviewed version available at Atmosphere 2020, 11, 177; doi:10.3390/atmos11020177

upwards. The cross section is located 2000km from the surface of the Earth. Out of 3000 echoing whistlers passing through that surface, we have picked 300 waves (interleaved by 10) to create the frequency time spectrogram in Figure 8. The frequency dispersion visible with lightning generated echoing whistlers can be seen in Figure 8, but that pattern disappears after 10 seconds. From there onward, there is no distinguishable pattern observed and the data points are distributed randomly creating a hiss-like pattern.

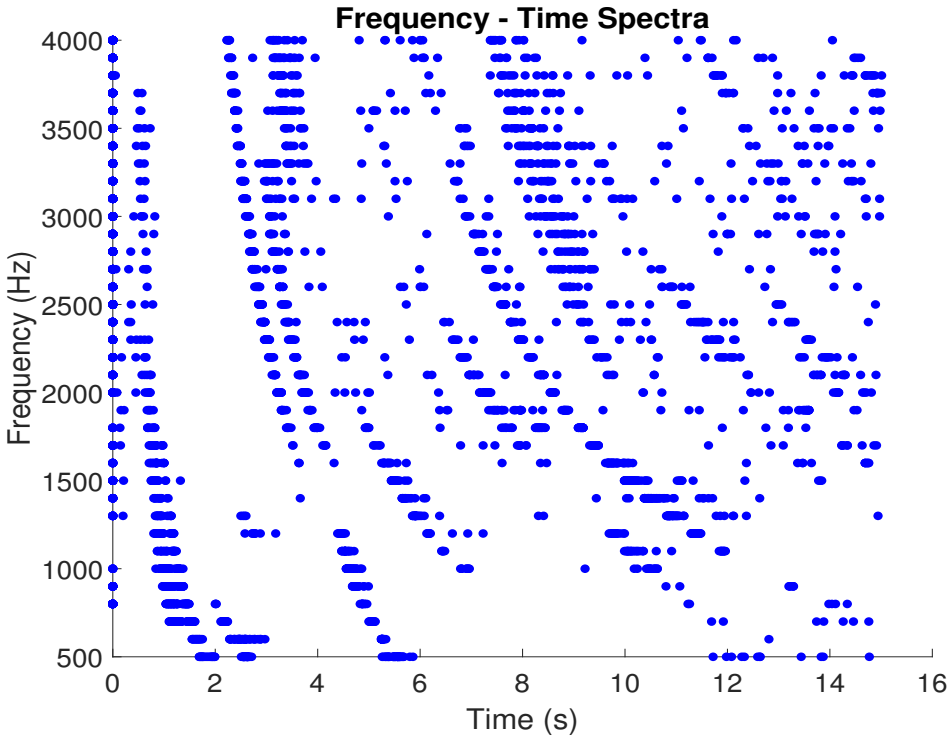

Figure 7. Frequency-time spectrogram of waves passing through a 1200km $\times$ 1200km section extending from equator, and located 2000km away from the surface of the Earth. Out of all the waves passing though this surface only 300 waves were used to plot this spectrogram to show that the initial frequency dispersion observed with whistlers disappears after about 10 seconds and the observation becomes more random and hiss-like.

5. Discussion

In early 1990', researchers predicted multiple reflections of lightning generated whistlers can be a possible source of hiss Draganov *et al.* [23], Sonwalkar and Inan [24] Their conclusion was based on the wave normal analysis, which showed low ($< 40^\circ$) wave normal angles for whistlers and as whistlers bounce between the two hemispheres, the wave normal angle become broad and more hiss-like. The observed wave normal angle for hiss waves were around 70°. We tried to re-produce this observation with our raytracing study. (It is worth noting here that ePOP-RRI cannot measure the wave normal angles.)

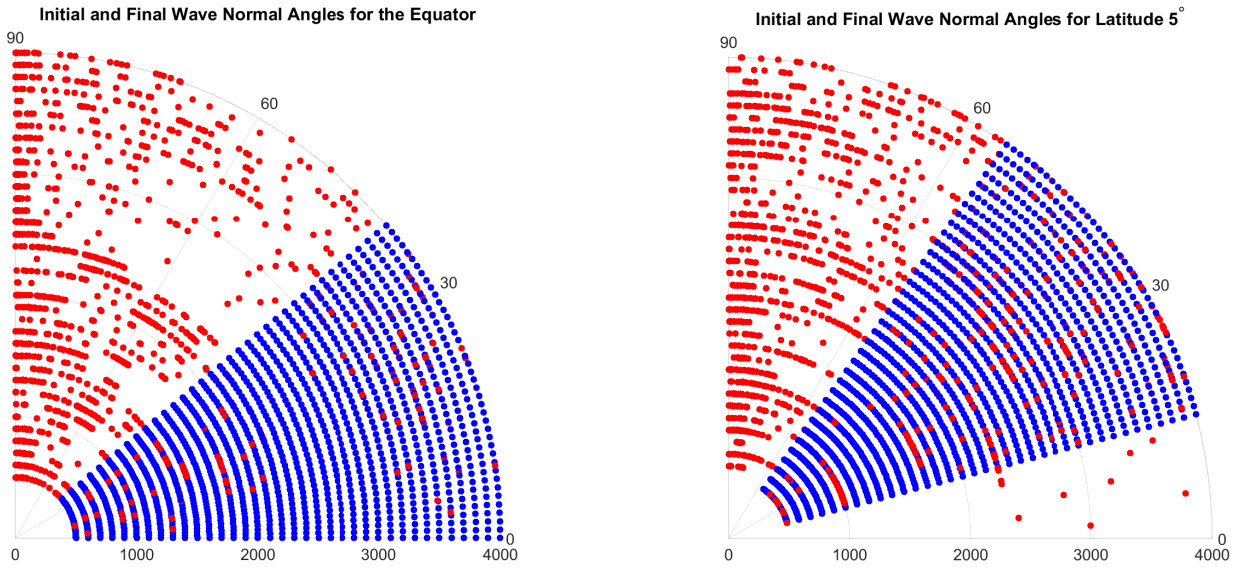

(a) (b)

Figure 8. In both figures, initial wave normal angles are indicated in blue and the final values are in red. Figure (a) shows the initial and final wave normal angles for the waves launched at the equator and (b) shows the initial and final wave normal angles for the latitude 5° launches. In both cases, the near-parallel wave normal angles change to more oblique values as wave prpagates. In otherwords the whislter wave normal angles become more hiss-like wave normal angles.

Figure 8, shows the results from the raytracing study. Blue markers represent initial wave normal angles and red markers show the final wave normal angles for launches from the equator and from latitude 5°. The initial wave normal angles resemble whistler wave normal angles and the final wave normal angles are more oblique representing hiss. Our wave normal angle simulation results agree with the raytracing studies and observations of Draganov *et al.* [23], Sonwalkar and Inan [24]. Based on the spectrograms, eccentricity studies and raytracing studies, we can support the argument that lightning generated whistlers can be a possible source of whistler mode hiss in the plasmasphere.

Majority of the hiss energy is observed between $L = 3$ and 4 [24]. In Table A1, we have indicated the L value of our observations, and those are shown in Figure 9. For the observations made between latitudes $\pm 20^\circ$, there were no L shell mappings, because of the diffusive region. According to Figure 9, majority of our hiss observations were made between $3 < L < 4$ agreeing with the previous observations.

Preprints (www.preprints.org) | NOT PEER-REVIEWED | Posted: 11 January 2020 doi:10.20944/preprints202001.0103.v1

Peer-reviewed version available at Atmosphere 2020, 11, 177; doi:10.3390/atmos11020177

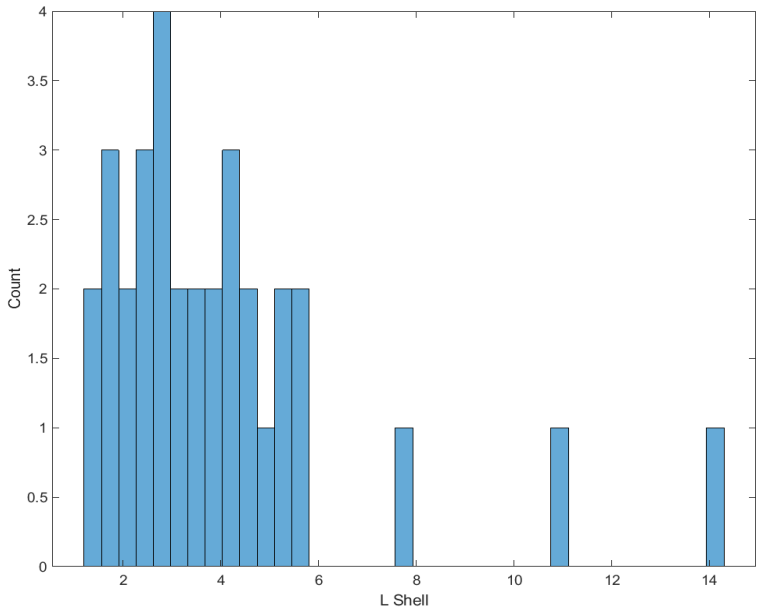

Figure 9. Occurrence of hiss with respect to the L value is shown in this figure. Majority of the observations were made with $L = 3 - 4$.

We also observed the lower hybrid resonance frequency and LH noise in our observations. Our observations show a close correlation between the occurrence of whistlers and the occurrence of LH emissions. Both LH frequency and whistlers are triggered by lightning strikes therefore, when there is higher lightning activity, there is a high probability of generating both whistlers and LH waves. Interaction between high intensity whistlers and LH waves, increases the noise level above the LH frequency. In the presence of strong LH noise, the amount of whistler energy reaching frequencies lower than LH frequency is low. With each bounce whistlers lose energy due to the interaction with LH noise. Hence there is less whistler energy to form the hiss-band. A future topic of interest would be the probability of whistlers forming the hiss band, in the presence of strong LH noise. The results of such a study would shed light in determining whether whistlers are a source of hiss.

Lower hybrid frequency is depended on electron, ion density and temperature. Therefore, these observations would be useful in determining plasma parameters based on LH frequency.

6. Conclusions

In this work we presented the observations of Radio Receiver Instrument (RRI) on the Enhanced Polar Outflow Probe (e—POP or SWARM —E). According to our observations, 51% of the time whistler mode hiss coexist with whistlers. Out of those 75 cases 70% of the time we observed the lower hybrid resonance as well. We presented multiple cases where whistlers co-existing with hiss, whistlers forming the hiss band, whistlers and LH without hiss and hiss in the absence of whistlers. Our observations suggested a strong probability of observing whistlers, LH and hiss simultaneously.

Our eccentricity analysis for hiss showed no difference in eccentricity between different cases. Main conclusion made here was that multiple echoes of ducted whistlers show a close resemblance of high frequency hiss. Frequency-time spectrogram produced from our raytracing study also suggested that whistlers show a more hiss-like behavior after multiple reflections. Which supports the idea of whistlers being a possible source of hiss.

Strong interactions between whistlers and LH noise was also observed. The stronger the interaction between whistlers and LH noise, less energy was observed below LH, hence LH frequency was acting as a ‘noise-filter’. LH noise gets amplified due to interactions with high intensity whistlers

and other lightning generated waves, therefore, higher the lightning activity, there is a high probability of observing whistlers and LH frequency.

7. Materials and Methods

All data used in this paper are publicly available from the e—POP data repository at https://epop-data.phys.ucalgary.ca/. Observation data were analyzed with MATLAB and the scripts will be available upon request. Raytracing simulations were performed using the Stanford 3D raytracer, which was developed at Stanford University and later modified to include warm plasma corrections at University of Colorado Denver. Access to the 3D raytracer will also be available upon request.

Author Contributions: Conceptualization, A.M, M.G and G.H, methodology M.G and A.M, data curation and software, A.M, writing–original draft preparation A.M and M.G, writing–review and editing, A.M, M.G and G.H, funding acquisition G.H and M.G

Funding: This research was funded by Canadian Space Agency under grant 16SUSTSSPI, e-POP/SWARM-E satellite mission is funded by Natural Science and Engineering Research Council under Discovery Grant RGPIN/06069-2014, and the European Space Agency (ESA) under the Third Party Mission Program. MG is funded by National Aeronautics and Space Administration(NASA) grant 80NSSC19K0264

Acknowledgments: Authors would like to acknowledge Dr. Andrew Yau at University of Calgary, a principal investigator of e-POP.

Conflicts of Interest: The authors declare no conflict of interest.

Abbreviations

The following abbreviations are used in this manuscript:

RRI	Radio Receiver Instrument
e-POP	Enhanced Polar Outflow Probe
GCPM	Global Core Plasmasphere Model

Appendix A

Appendix A.1

Table A1. List of events in which whistlers were observed and indicating whether the hiss and or the lower hybrid resonance was observed too.

Number	Date	Pass Start Time (UT)	Altitude (km)	L-shell	Ducted?	Hiss?	LHR?
1	2014-Feb-19	14:29:14	600	2.72	Y	Y	Y
2	2014-Feb-22	14:29:14	500	5.34	Y	N	Y
3	2014-Aug-03	03:49:09	884	4.49	Y	Y	Y
4	2014-Oct-11	02:43:08	1282	2.60	Y	N	N
5	2015-May-19	22:14:44	443	5.35	Y	Y	Y
6	2015-Jun-19	00:17:44	553	3.26	Y	Y	Y
7	2015-Jun-29	06:36:14	800	4.79	Y	Y	Y
8	2015-Jul-03	05:44:13	950	5.32	Y	N	N
9	2016-Jan-17	13:23:04	877	2.04	N	N	N
10	2016-Jan-22	20:11:04	500	1.51	N	N	N
11	2016-Mar-08	14:00:29	1352	2.17	N	N	N
12	2016-Oct-21	10:18:44	836	3.92	Y	Y	Y
13	2017-Jun-13	00:14:44	358	3.59	Y	N	Y
14	2017-Jun-21	04:02:14	477	5.53	Y	Y	Y
15	2017-Jun-22	18:58:14	633	5.10	Y	Y	Y
16	2018-Mar-07	15:19:44	651	2.60	N	N	Y
17	2018-Mar-10	11:37:44	1150	1.65	N	N	Y
18	2018-Mar-12	14:59:13	530	2.37	N	N	Y
19	2018-Mar-13	00:50:43	900	–	N	Y	Y
20	2018-Apr-28	21:30:14	1300	3.85	N	N	Y
21	2018-Apr-30	19:00:14	1311	4.18	N	N	Y
22	2018-May-10	09:08:14	550	14.29	N	Y	Y
23	2018-May-12	15:36:14	1300	–	N	N	Y
24	2018-May-13	15:11:44	1300	1.60	N	Y	Y
25	2018-May-14	06:00:44	1057	2.42	N	Y	Y
26	2018-May-15	03:53:44	1074	2.90	N	Y	Y
27	2018-May-19	05:37:44	1140	2.86	N	Y	Y
28	2018-May-19	14:24:44	1260	1.59	N	Y	Y
29	2018-May-24	01:50:14	1250	2.33	N	Y	Y
30	2018-May-25	01:25:14	1260	2.28	N	Y	Y
31	2018-Jun-04	09:47:14	381	3.41	Y	Y	Y
32	2018-Jun-19	05:09:44	370	4.15	Y	Y	N
33	2018-Jun-20	04:44:48	380	3.72	Y	Y	Y
34	2018-Jun-20	06:24:42	350	7.77	Y	Y	Y
35	2018-Jun-29	02:40:47	372	5.47	Y	Y	N
36	2018-Jun-30	00:35:44	373	4.36	N	Y	N
37	2018-Jun-30	02:15:46	500	4.36	N	Y	N
38	2018-Jul-14	23:25:41	928	4.21	Y	N	Y
39	2018-Jul-21	00:42:15	1290	–	N	Y	Y
40	2018-Jul-21	07:10:15	1128	1.94	Y	Y	Y
41	2018-Jul-21	22:50:45	1096	1.92	N	Y	N
42	2018-Jul-22	06:48:45	1190	1.70	N	Y	Y
43	2018-Jul-22	08:43:45	1285	–	N	Y	N
44	2018-Jul-22	23:52:15	1286	–	N	Y	Y
45	2018-Jul-23	06:23:45	1228	1.53	N	Y	Y

Table A2. List of events in which whistlers were observed and indicating whether the hiss and or the lower hybrid resonance was observed too.

Number	Date	Pass Start Time (UT)	Altitude (km)	L-shell	Ducted?	Hiss?	LHR?
46	2018-Jul-23	08:18:45	1277	–	N	Y	N
47	2018-Jul-24	07:53:44	1270	–	N	N	N
48	2018-Jul-27	21:31:17	1225	4.12	Y	N	Y
49	2018-Jul-28	08:08:15	785	10.87	N	Y	Y
50	2018-Jul-28	21:05:17	1264	3.47	Y	Y	Y
51	2018-Jul-28	22:46:47	1269	2.93	Y	N	Y
52	2018-Aug-10	06:01:45	660	2.56	N	N	Y
53	2018-Aug-12	06:52:15	563	3.23	N	N	Y
54	2018-Aug-13	06:26:45	570	2.78	N	Y	Y
55	2018-Aug-14	09:15:15	736	1.25	N	N	N
56	2018-Aug-26	22:32:15	800	1.28	Y	Y	Y
57	2018-Aug-29	04:45:45	336	3.25	Y	N	Y
58	2018-Aug-30	04:19:15	335	3.03	N	N	Y
59	2018-Sep-01	03:27:45	331	2.82	N	N	Y
60	2018-Oct-05	09:32:14	1293	2.72	N	N	Y
61	2018-Oct-07	08:41:14	1291	3.35	Y	Y	Y
62	2018-Oct-10	09:05:13	1259	2.58	Y	N	Y
63	2018-Oct-11	08:39:13	1240	2.46	N	N	Y
64	2018-Oct-12	08:13:14	1240	2.78	N	N	Y
65	2018-Oct-13	07:48:14	1240	3.06	N	N	Y
66	2018-Oct-14	09:05:14	1235	3.09	Y	Y	Y
67	2018-Oct-15	08:38:14	1206	2.70	N	N	Y
68	2018-Oct-16	08:12:14	1180	2.57	N	N	Y
69	2018-Oct-20	08:12:14	1135	2.82	Y	N	Y
70	2018-Oct-21	07:45:14	1090	2.59	Y	N	Y
71	2018-Oct-22	07:20:14	1107	3.26	N	N	Y
72	2018-Oct-26	07:18:14	977	2.51	Y	N	N
73	2018-Oct-28	06:26:14	1033	4.5	Y	Y	N
74	2018-Nov-07	05:33:14	650	2.05	N	N	N
75	2018-Dec-26	22:21:44	616	–	N	N	N
	Total	75				39	57
	Percentage	%				52	76

References

1. Bortnik, J.; Thorne, R.M.; Meredith, N.P. Modeling the propagation characteristics of chorus using CRRES suprathermal electron fluxes. *Journal of Geophysical Research: Space Physics* **2007**, *112*. doi:10.1029/2006JA012237.
2. Horne, R.B.; Thorne, R.M. Potential waves for relativistic electron scattering and stochastic acceleration during magnetic storms. *Geophysical Research Letters* **1998**, *25*, 3011–3014. doi:10.1029/98GL01002.
3. Horne, R.B.; Meredith, N.P.; Thorne, R.M.; Heynderickx, D.; Iles, R.H.A.; Anderson, R.R. Evolution of energetic electron pitch angle distributions during storm time electron acceleration to megaelectronvolt energies. *Journal of Geophysical Research: Space Physics* **2003**, *108*. doi:10.1029/2001JA009165.
4. Horne, R.B.; Thorne, R.M.; Glauert, S.A.; Albert, J.M.; Meredith, N.P.; Anderson, R.R. Timescale for radiation belt electron acceleration by whistler mode chorus waves. *Journal of Geophysical Research: Space Physics* **2005**, *110*. doi:10.1029/2004JA010811.
5. Lyons, L.R.; Lee, D.Y.; Thorne, R.M.; Horne, R.B.; Smith, A.J. Solar wind-magnetosphere coupling leading to relativistic electron energization during high-speed streams. *Journal of Geophysical Research: Space Physics* **2005**, *110*. doi:10.1029/2005JA011254.
6. Meredith, N.P.R.B.H.; Clilverd, M.A.; Horsfall, D.; Thorne, R.M.; Anderson, R.R. Origins of plasmaspheric hiss. *Geophys. Res.* **2006**, *111, A09217*. doi:10.1029/2006JA011707.

7. Miyoshi, Y.; Morioka, A.; H.Misawa.; Obara, T.; T.Nagai.; Kasahara, Y. Rebuilding process of the outer radiation belt during the 3 November 1993 magnetic storm: NOAA and Exos-D observations. *Journal of Geophysical Research: Space Physics* **2003**, *108*. doi:10.1029/2001JA007542.
8. Nakamura, S.; Omura, Y.; Summers, D.; Kletzing, C.A. Observational evidence of the nonlinear wave growth theory of plasmaspheric hiss. *Geophysical Research Letters* **2016**, *43*, 10,040–10,049. doi:10.1002/2016GL070333.
9. Smith, A.J.; Horne, R.B.; Meredith, N.P. Ground observations of chorus following geomagnetic storms. *Journal of Geophysical Research: Space Physics* **2004**, *109*. doi:10.1029/2003JA010204.
10. Spasojevíc, M.; Inan, U.S. Ground based VLF observations near L = 2.5 during the Halloween 2003 storm. *Geophysical Research Letters* **2005**, *32*. doi:10.1029/2005GL024377.
11. Summers, D.; Thorne, R.M.; Xiao, F. Relativistic theory of wave-particle resonant diffusion with application to electron acceleration in the magnetosphere. *Journal of Geophysical Research: Space Physics* **1998**, *103*, 20487–20500. doi:10.1029/98JA01740.
12. Thorne, R.M.; O'Brien, T.P.; Shprits, Y.Y.; Summers, D.; Horne, R.B. Timescale for MeV electron microburst loss during geomagnetic storms. *Journal of Geophysical Research: Space Physics* **2005**, *110*. doi:10.1029/2004JA010882.
13. Varotsou, A.; Boscher, D.; Bourdarie, S.; Horne, R.B.; Glauert, S.A.; Meredith, N.P. Simulation of the outer radiation belt electrons near geosynchronous orbit including both radial diffusion and resonant interaction with Whistler-mode chorus waves. *Geophysical Research Letters* **2005**, *32*. doi:10.1029/2005GL023282.
14. Wang, C., a.Q.Z.; F. Xiao, a.Z.S.; Wang, Y.; Yue, C. The relations between magnetospheric chorus and hiss inside and outside the plasmasphere boundary layer: Cluster observation. *Geophys. Res.* **2011**, *116, A07221*. doi:10.1029/2010JA016240.
15. Gołkowski, M.; Inan, U.S. Multistation observations of ELF/VLF whistler mode chorus. *Journal of Geophysical Research: Space Physics* **2008**, *113*.
16. Hosseini, P.; Gołkowski, M.; Turner, D.L. Unique concurrent observations of whistler mode hiss, chorus, and triggered emissions. *Journal of Geophysical Research: Space Physics* **2017**, *122*, 6271–6282. doi:10.1002/2017JA024072.
17. Lyons, L.R.; Thorne, R.M. Equilibrium structure of radiation belt electrons. *Journal of Geophysical Research (1896-1977)* **1973**, *78*, 2142–2149. doi:10.1029/JA078i013p02142.
18. Omura, Y.; Hikishima, M.; Katoh, Y.; Summers, D.; Yagitani, S. Nonlinear mechanisms of lower-band and upper-band VLF chorus emissions in the magnetosphere. *Journal of Geophysical Research: Space Physics* **2009**, *114*. doi:10.1029/2009JA014206.
19. Omura, Y.; Nunn, D. Triggering process of whistler mode chorus emissions in the magnetosphere. *Journal of Geophysical Research: Space Physics* **2011**, *116*. doi:10.1029/2010JA016280.
20. Gołkowski, M.; Gibby, A.R. On the conditions for nonlinear growth in magnetospheric chorus and triggered emissions. *Physics of Plasmas* **2017**, *24*, 092904. doi:10.1063/1.4986225.
21. Gołkowski, M.; Harid, V.; Hosseini, P. Review of Controlled Excitation of Non-linear Wave-Particle Interactions in the Magnetosphere. *Frontiers in Astronomy and Space Sciences* **2019**, *6*, 2. doi:10.3389/fspas.2019.00002.
22. Smith, R.L.; Angerami, J.J. Magnetospheric properties deduced from OGO 1 observations of ducted and nonducted whistlers. *Geophys. Res.* **1968**, *73, 1*.
23. Draganov, A.B.U.S.I.; Sonwalkar, V.S.; Bell, T.F. Whistlers and plasmaspheric hiss: Wave directions and three-dimensional propagation. *Geophys. Res.* **1993**, *98, 11,401*.
24. Sonwalkar, V.; Inan, U. Lightning as an embryonic source of VLF hiss. *Journal of Geophysical Research: Space Physics* **1989**, *94*, 6986–6994. doi:10.1029/JA094iA06p06986.
25. Omura, Y.; Nakamura, S.; Kletzing, C.A.; Summers, D.; Hikishima, M. Nonlinear wave growth theory of coherent hiss emissions in the plasmasphere. *Journal of Geophysical Research: Space Physics* **2015**, *120*, 7642–7657. doi:10.1002/2015JA021520.
26. Cornilleau-Wehrlin, N.; Gendrin, R.; Lefeuvre, F.; Parrot, M.; Grard, R.; Jones, D.; Bahnsen, A.; Ungstrup, E.; Gibbons, W. VLF electromagnetic waves observed onboard GEOS-1. *Space Sci. Rev.* **1978**, *22*, 371–382.
27. Hayakawa, M.; Ohmi, N.; Parrot, M.; Lefeuvre, F. Direction finding of ELF hiss emissions in a detached plasma region of the magnetosphere. *Geophys. Res.* **1986**, *91(A1)*, 135–141.

28. Parrot, M.; Lefeuvre, F. Statistical study of the propagation characteristics of ELF hiss observed on GEOS-1, inside and outside the plasmasphere. *Ann. Geophys., Ser* **1986**, *A, 4*, 363–384.
29. Russell, C. T., R.E.H.; Smith, E.J. *OGO 3 observations of ELF noise in the magnetosphere: 1. Spatial extent and frequency of occurrence* **1969**, *74(3)*, 755–777.
30. Bortnik, J.; Thorne, R.; Meredith, N. The unexpected origin of plasmaspheric hiss from discrete chorus emissions. *nature* **2008**, *452*, 62–66. doi:10.1038/nature06741.
31. Bortnik, J.; Li, W.; Thorne, R.; Angelopoulos, V.; Cully, C.; Bonnell, J.; Le Contel, O.; Roux, A. An Observation Linking the Origin of Plasmaspheric Hiss to Discrete Chorus Emissions. *Science* **2009**, *324*, 775–778.
32. Bortnik, J.; Chen, L.; Li, W.; Thorne, R.; Horne, R.B. Modeling the evolution of chorus waves into plasmaspheric hiss. *Journal of Geophysical Research: Space Physics* **2011**, *116*.
33. Delport, B.A.B.C.; Lichtenberger, J.; Rodger, C.J.; Parrot, M.; Clilverd, M.A.; Friedel, R.H.W. Simultaneous observation of chorus and hiss near the plasmapause. *Geophys. Res.* **2012**, *117, A12218*. doi:10.1029/2012JA017609.
34. Hartley, D.P.; Kletzing, C.A.; Chen, L.; Horne, R.B.; Santolík, O. Van Allen Probes Observations of Chorus Wave Vector Orientations: Implications for the Chorus-to-Hiss Mechanism. *Geophysical Research Letters* **2019**, *46*, 2337–2346. doi:10.1029/2019GL082111.
35. Hosseini, P.; Gołkowski, M.; Harid, V. Remote sensing of radiation belt energetic electrons using lightning triggered upper band chorus. *Geophysical Research Letters* **2019**, *46*, 37–47.
36. Parrot, M.; Berthelier, J.J.; Lebreton, J.P.; Treumann, R.; Rauch, J.L. DEMETER Observations of EM Emissions Related to Thunderstorms. *Space Science Reviews* **2008**, *137*, 511–519. doi:10.1007/s11214-008-9347-y.
37. Parrot, M.; Nemec, F.; Santolik, O. Statistical analysis of VLF radio emissions triggered by power line harmonic radiation and observed by the low-altitude satellite DEMETER. *Journal of Geophysical Research: Space Physics* **2014**, *119*, 5744–5754.
38. Parrot, M.; Santolik, O.; Nemec, F. Chorus and chorus-like emissions seen by the ionospheric satellite DEMETER. *Journal of Geophysical Research: Space Physics* **2016**, *121*, 3781–3792.
39. Santolík, O.; Parrot, M.; Lefeuvre, F. Singular value decomposition methods for wave propagation analysis. *Radio Science* **2003**, *38*.
40. Santolik, O.; Gurnett, D.A.; Pickett, J.S.; Chum, J.; Cornilleau-Wehrlin, N. Oblique propagation of whistler mode waves in the chorus source region. *Journal of Geophysical Research: Space Physics* **2009**, *114*.
41. James, H.G.; King, E.P.; White, A.; Hum, R.H.; Lunscher, W.H.H.L.; Siefring, C.L. The e-POP Radio Receiver Instrument on CASSIOPE. *Space Science Reviews* **2015**, *189*, 79–105.
42. Perry, G.W.; James, H.G.; Gillies, R.G.; Howarth, A.; Hussey, G.C.; McWilliams, K.A.; White, A.; Yau, A.W. First results of HF radio science with e-POP RRI and SuperDARN. *Radio Science* **2017**, *52*, 78–93.
43. Danskin, D.W.; Hussey, G.C.; Gillies, R.G.; James, H.G.; Fairbairn, D.T.; Yau, A.W. Polarization Characteristics Inferred From the Radio Receiver Instrument on the Enhanced Polar Outflow Probe. *Journal of Geophysical Research: Space Physics* **2018**, *123*, 1648–1662.
44. Brice, N.; Smith, R. Recordings from Satellite Alouette I: A Very-low-frequency Plasma Resonance. *nature* **1964**, *203*. doi:10.1038/nature06741.
45. Brice, N.M.; Smith, R.L. Lower hybrid resonance emissions. *Journal of Geophysical Research (1896-1977)* **1965**, *70*, 71–80. doi:10.1029/JZ070i001p00071.
46. Lee, M.C.; Kuo, S.P. Production of lower hybrid waves and field-aligned plasma density striations by whistlers. *Journal of Geophysical Research: Space Physics* **1984**, *89*, 10873–10880. doi:10.1029/JA089iA12p10873.
47. Bell, T.F.; Inan, U.S.; Sonwalkar, V.S.; Helliwell, R.A. DE-1 observations of lower hybrid waves excited by VLF whistler mode waves. *Geophysical Research Letters* **1991**, *18*, 393–396.
48. Shklyar, D.R.; Washimi, H. Lower hybrid resonance wave excitation by whistlers in the magnetospheric plasma. *Journal of Geophysical Research: Space Physics* **1994**, *99*, 23695–23704.
49. Bell, T.; James, H.; Inan, U.; Katsufrakis, J. The apparent spectral broadening of VLF transmitter signals during transionospheric propagation. *Journal of Geophysical Research: Space Physics* **1983**, *88*, 4813–4840.
50. Born, M.; Wolf, E. *Principles of Optics: Electromagnetic Theory of Propagation, nterference and Diffraction of Light, 6th ed*; Pergamon Press: Oxford, United Kingdom, 1980.

366 51. Bass, M.; DeCusatis, C.; Enoch, J.; Lakshminarayanan, V.; Li, G.; Macdonald, C.; Mahajan, V.; Van Stryland,
367 E. *Handbook of Optics, Third Edition Volume I: Geometrical and Physical Optics, Polarized Light, Components and*
368 *Instruments(Set)*, 3 ed.; McGraw-Hill, Inc.: New York, NY, USA, 2010.